Front. Chem. Sci. Eng. 2018, 12(3): 417–424
https://doi.org/10.1007/s11705-018-1711-1

RESEARCH ARTICLE

3D Network nanostructured NiCoP nanosheets supported on N-doped carbon coated Ni foam as a highly active bifunctional electrocatalyst for hydrogen and oxygen evolution reactions

Miaomiao Tong, Lei Wang (✉), Peng Yu, Xu Liu, Honggang Fu (✉)

Key Laboratory of Functional Inorganic Material Chemistry, Ministry of Education of the People's Republic of China, Heilongjiang University, Harbin 150080, China

Abstract A highly active bi-functional electrocatalyst towards both hydrogen and oxygen evolution reactions is critical for the water splitting. Herein, a self-supported electrode composed of 3D network nanostructured NiCoP nanosheets grown on N-doped carbon coated Ni foam (NiCoP/NF@NC) has been synthesized by a hydrothermal route and a subsequent phosphorization process. As a bifunctional electrocatalyst, the NiCoP/NF@NC electrode needs overpotentials of 31.8 mV for hydrogen evolution reaction and 308.2 mV for oxygen evolution reaction to achieve the current density of 10 mA·cm^{-2} in 1 mol·L^{-1} KOH electrolyte. This is much better than the corresponding monometal catalysts of CoP/NF@NC and NiP/NF@NC owing to the synergistic effect. NiCoP/NF@NC also exhibits low Tafel slope, and excellent long-term stability, which are comparable to the commercial noble catalysts of Pt/C and RuO_2.

Keywords bimetallic phosphides, N-doped carbon, self-support, hydrogen evolution, oxygen evolution

1 Introduction

With the growing concern of energy crisis and global warming [1,2], the need for exploration of novel energy sources to replace the ever-being-exhausted tradition fossil fuels is a top priority [3,4]. Hydrogen is a promising alternative due to its environmental friendliness and recyclability [5]. Nowadays, electrochemical water splitting has been widely regarded as an efficient and environmentally friendly technology for producing hydrogen energy [6–10]. However, the cathodic hydrogen evolution reaction (HER) and anodic oxygen evolution reaction (OER), two vital half reactions of water electrolysis, are kinetically sluggish. Although Pt-based [11] and IrO_2/RuO_2-based [12] catalysts, which are the state-of-the-art catalysts towards HER and OER, respectively, can reduce the overpotential to drive the reactions, their further application is limited from a long-term perspective due to the scarcity and high-cost nature of noble metals. Besides, these catalysts could not satisfy the bifunctional electrocatalysis for both HER and OER [13–17]. Accordingly, it is highly desirable to develop an alternative, low-cost, and efficient electrocatalyst for water splitting [18–20] with the highest possible energy efficiency by reducing overpotentials.

Recently, considerable efforts have been devoted to non-noble metal compounds such as transition metal nitrides (FeN, Co_4N) [21–23], carbides (Mo_2C) [24], sulphides (CoS_2, MoS_2) [25–28], selenides (WSe_2, $MoSe_2$) [29–32] and borides (Mo_2B_4) [33] as HER and/or OER electrocatalysts because of the low cost. Transition-metal phosphides have also drawn much attention because they show much better performance than the other bifunctional electrocatalysts towards HER and OER. Bimetallic-structured phosphide such as $NiCo_xP_y$ [34–40] could exhibit better HER and OER performances than the corresponding monometal phosphides (CoP and NiP) [41] owing to the synergistic effect. Moreover, the microstructure and morphology of electrocatalysts directly affect their active sites and catalytic performance. Three-dimensional (3D) network structures have attracted a tremendous amount of attention because the abundant interior space and large surface areas could be responsible for fast diffusion of ions and enhanced reaction kinetics. Undoubtedly, the use of self-supported substrates (such as Ni foam) is the most effective and facile strategy for

Received December 30, 2017; accepted February 4, 2018

E-mails: wanglei0525@126.com (Wang L), fuhg@vip.sina.com (Fu H)

synthesis of the special 3D network nanostructures [42–44]. Moreover, the introduction of N-doped carbon nanostructures could enhance the catalytic properties due to the asymmetrical electron spin density and charge polarization produced by the electronegativity difference between carbon and N atoms. Besides, the carbon nanostructures could improve the dispersion and stability of metal phosphides. Therefore, the effective combination of NiCoP and N-doped nanostructures on Ni foam may be an effective strategy to prepare the HER and OER bifunctional electrocatalyst.

Herein we have constructed a self-supported electrode composed of 3D network nanostructured NiCoP grown on N-doped carbon coated Ni foam (NiCoP/NF@NC) by a hydrothermal route and a subsequent phosphorization process.

2 Experimental

2.1 Synthesis of NiCoP/NF@NC

NiCoP/NF@NC was prepared by a simple hydrothermal and a subsequent carbonized route. A piece of NF (3×4 cm^2) was firstly soaked in 2 mol·L^{-1} HCl solution for 20 min to remove the oxide layer. After washed with deionized water and acetone, the NF was dried for standby application. In a typical synthesis, the pre-treated NF was soaked in a 5% dopamine aqueous solution for 20 min to obtain the dopamine coated NF sample. The coated NF was then heated at 900 °C for 2 h under N_2 to afford the N-doped carbon coated NF (namely NF@NC). Subsequently, Ni$(NO_3)_2 \cdot 6H_2O$ (4 mmol) and 2 mmol $Co(NO_3)_2 \cdot 6H_2O$ (2 mmol) were dissolved into deionized water (40 mL) and stirred for 10 min. Then an aqueous solution (20 mL) composed of NH_4F (18 mmol) and urea (6 mmol) was poured into the above solution and stirred for 5 min. The resulting solution was transferred into a Teflon-lined stainless autoclave (100 mL) and reacted with NF@NC at 120 °C for 8 h. The resulting product, named as NiCo/NF@NC, was washed with deionized water for several times and then dried in vacuum at 60 °C for 6 h. To prepare the phosphides, $NaH_2PO_2 \cdot H_2O$ (1.5 g) was placed at the upstream side of the tube furnace and the NiCo/NF@NC was placed at the downstream side. The sample was heated at 350 °C for 3 h with an Ar gas flow at a flowrate of 40 mL·min^{-1} to produce NiCoP/NF@NC. As compared, the Ni/NF@NC and Co/NF@NC samples were also prepared by the similar procedure.

2.2 Characterizations

X-ray diffraction (XRD, Rigaku D/max-IIIB, Bruker) was used to analyze the crystalline structures. Scanning electron microscopy (SEM, Hitachi S-4800) and (TEM, JEOL JEM-2100) were used to characterize the microstructures. The composition was determined by X-ray photoelectron spectroscopy (XPS, VG ESCALABMK II).

2.3 Electrochemical tests

All OER and HER activities were investigated by a standard three-electrode system on CHI660 electrochemical workstation in a 1.0 mol·L^{-1} KOH electrolyte. The prepared NiCoP/NF@NC composite was adopted as a working electrode, a graphite rod served as a counter electrode and a saturated calomel electrode (SCE) were used as a reference electrode. The current density was normalized to the geometrical area. The measured potential was calibrated with RHE according to the formula in 1.0 mol·L^{-1} KOH electrolyte and the following equation: E(RHE) = E(SCE) + 1.059 V.

The HER and OER performances were tested in N_2 and O_2-saturated 1.0 mol·L^{-1} KOH electrolytes, respectively. Cyclic voltammetry was run at least for 50 cycles at 50 mV·s^{-1} to completely stabilize the catalyst before recoding the data. Polarization curves were performed by using linear sweep voltammetry (LSV) at a scan rate of 5 mV·s^{-1}. Electrochemical double-layer capacitances (C_{dl}) were determined by cyclic voltammetry at a scan rate of 20–200 mV·s^{-1}. In the test of stability performance, cyclic voltammetry (CV) scan at a rate of 50 mV·s^{-1} was performed in 1.0 mol·L^{-1} KOH electrolyte for 10000 cycles, then the LSV curve was recorded. The average total mass-loading on the NF substrate was about 2.7 mg·cm^{-2}, with loadings of NiCoP and N-doped carbon being about 1.2 and 1.5 mg·cm^{-2}, respectively.

3 Results and discussion

The NiCoP/NF@NC was synthesized by a hydrothermal and phosphorization process. Firstly, the Ni foam was coated with N-doped carbon to prepare NF@NC by using dopamine as the N resource. Then, the NiCo/NF@NC precursor could be prepared by a hydrothermal route. The crystal structure of each process is confirmed by XRD as shown in Fig. 1. The NiCo/NF@NC exhibits the main crystalline phase of $NiCo_2O_4$ (PDF#20-0781). The Ni characteristic peaks should be originated from the Ni foam substrate. After phosphorization, $NiCo_2O_4$ was converted to NiCoP (PDF#71-2336) as evidenced by XRD, so the NiCoP/NF@NC was obtained. As compared, the CoP/NF@NC and NiP/NF@NC were also prepared without using $Ni(NO_3)_2 \cdot 6H_2O$ and $Co(NO_3)_2 \cdot 6H_2O$, respectively. It can be seen that CoP_2 (PDF#26-0481) and Ni_5P_4 (PDF#18-0883) exhibit in CoP/NF@NC and NiP/NF@NC, respectively.

Microstructures and morphologies of NiCoP/NF@NC were further investigated by SEM and TEM. As shown in

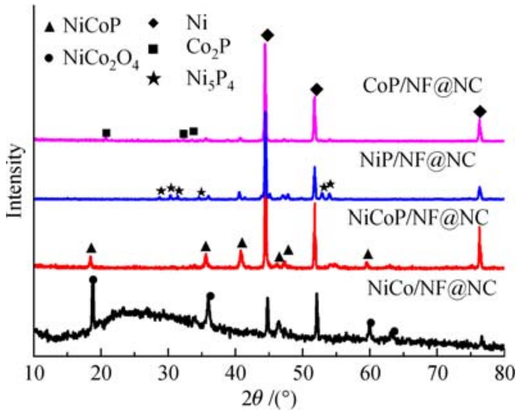

Fig. 1 XRD patterns of NiCo/NF@NC, NiCoP/NF@NC, CoP/NF@NC and NiP/NF@NC

Fig. 2(A), Ni foam is uniformly covered by 3D network structured NiCoP nanosheets. The enlarged SEM images (Figs. 2(B,C)) further show that the surface of nanosheets is rough, which could increase the active sites and facilitate the ion diffusion. Figure 2(D) shows a representative TEM image of NiCoP nanosheets shaved off from NiCoP/NF@NC. A carbon layer with a thickness of 8−10 nm coated on the NiCoP nanosheets was observed (Fig. 2(E)). The HRTEM image in Fig. 2(F) displays a lattice spacing of 0.22 nm, corresponding to the (111) interplanar spacings of hexagonal NiCoP.

XPS was used to further analyze the composition and surface structure of NiCoP/NF@NC. The XPS survey spectra in Fig. 3(A) shows that Ni, Co, P, N, C and O coexist in the NiCoP/NF@NC. The high-resolution spectra were further used to analyze the valences of Ni 2p, Co 2p, P 2p, N 1s and C 1s. As shown in Fig. 3(B), the Ni 2p3/2 energy level peak at 853.1 eV is attributed to Ni^{d+} in NiCoP, whereas the peak at 856.9 eV is originated from Ni oxide species. In the Ni 2p1/2 energy level, the peaks at 870.3 and 875.2 eV correspond to the Ni^{d+} in NiCoP and Ni oxide species, respectively. The other two peaks at 862.2 and 881.1 eV are ascribed to the satellites of the Ni 2p3/2 and Ni 2p1/2, respectively [45]. For Co 2p spectra (Fig. 3(C)), peaks at 778.6 and 782.2 eV belong to Co^{3+} and Co^{2+} of Co 2p3/2, respectively, which originated from Co–P and Co oxidized state. In the Co 2p1/2 energy level, the peaks at 798.5 and 801.7 eV are assigned to Co^{3+} and Co^{2+}, respectively. Moreover, the peaks at 786.4 and 804.4 eV could be assigned to the satellite peaks of Co 2p3/2 and Co 2p1/2 [45]. For P 2p XPS spectra in Fig. 3(D), the two peaks at 129.4 and 130.5 eV belongs to P 2p3/2 and P 2p1/2, respectively, derived from NiCoP. The peak at 134.8 eV corresponds to phosphate radical or P_2O_5 [45]. The above results demonstrate the main phase is NiCoP, and some oxidized species also exist due to surface oxidation of NiCoP. The N 1s XPS spectrum can be deconvoluted to pyridinic N at 397.5 eV, pyrrolic N at 399.2 eV and graphitic nitrogen atoms doped in the carbon matrix at 402.9 eV (Fig. 3(E)), which are favorable for the electrocatalytic performance [45]. Figure 3(F) displays the XPS of the C 1s; the peaks at 284.6, 285.9 and 288.7 eV correspond to the C = C, C–N and –C–O, respectively. The existence of C–N bond further indicated the successful doping of nitrogen in the carbon matrix [46,47].

The HER catalytic performance was first investigated by a three-electrode system in 1.0 $mol\cdot L^{-1}$ KOH electrolyte.

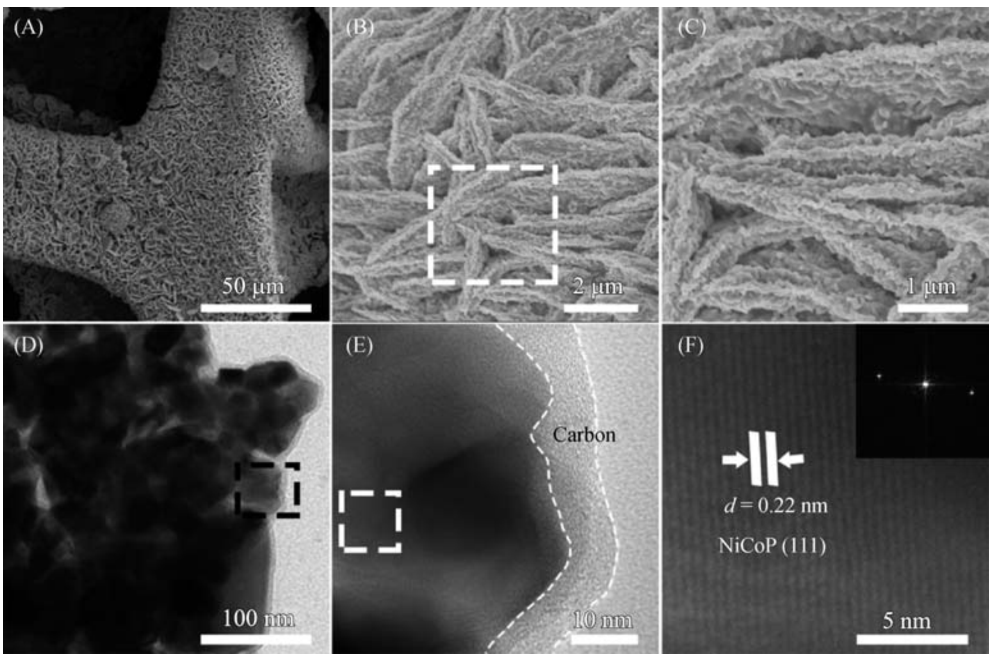

Fig. 2 (A−C) SEM, (D) TEM and (E, F) HRTEM images of NiCoP/NF@NC

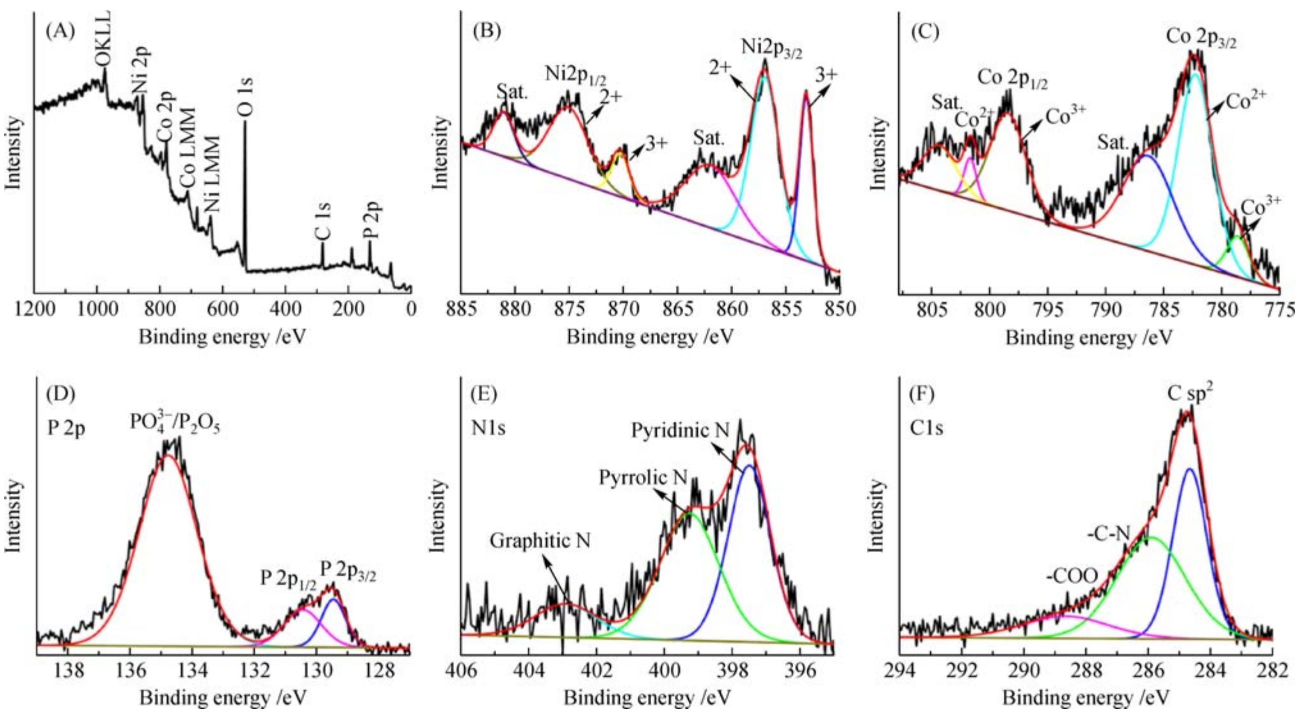

Fig. 3 (A) Wide XPS spectra of NiCoP/NF@NC; high-resolution XPS spectra of (B) Ni 2p, (C) Co 2p, (D) P 2p, (E) N 1s and (F) C 1s for NiCoP/NF@NC

As compared, the NiP/NF@NC and CoP/NF@NC were also tested. Similarly, the commercial 20% Pt/C catalyst and NiCoP powder were coated on NF@NC for comparison, respectively, named as Pt/C-NF@NC and NiCoP-NF@NC. Polarization curves were obtained from linear sweeping voltammetry (LSV) at a sweeping rate of 5 $mV\cdot s^{-1}$ as shown in Fig. 4(A). The NiCoP/NF@NC shows an overpotential of 31.8 mV at the current density of 10 $mA\cdot cm^{-2}$, whereas Pt/C-NF@NC needs an overpotential of 10.5 mV to achieve the same current density (Table S1). However, the overpotential of NiCoP-NF@NC at the current density of 10 $mA\cdot cm^{-2}$ is much higher than those of the NiP/NF@NC (126.6 mV) and CoP/NF@NC (112.1 mV), indicating the HER activity of NiCoP-NF@NC is much better than that of the corresponding monometal phosphide owing to the synergistic effect. Moreover, the overpotential of NiCoP/NF@NC electrode at 10 $mA\cdot cm^{-2}$ is much lower than that of the NiCoP-NF@NC electrode (279.3 mV). It is attributed to the intimate contact between NiCoP and NF@NC substrate originated from the *in-situ* growth strategy to facilitate the transfer of electron and ions.

The Tafel plot, overpotential *versus* log (j), is always applied to reveal the catalytic mechanism of HER. The Tafel slope for NiCoP/NF@NC is 62.3 $mV\cdot dec^{-1}$, which suggesting that the electrochemical desorption Heyrovsky step is the rate-determining step and the NiCoP/NF@NC as electrocatalyst for HER follows a Volmer-Heyrovsky mechanism ($H_2O + e^- = H_{ads} + OH^-$, $H_2O + e^- + H_{ads} = H_2 + OH^-$). The Tafel slope of NiCoP/NF@NC is much less than those of NiP/NF@NC (80.1 $mV\cdot dec^{-1}$), CoP/NF@NC (77.8 $mV\cdot dec^{-1}$) and NiCoP-NF@NC (109.6 $mV\cdot dec^{-1}$), implying the more favorable catalytic kinetics of NiCoP/NF@NC towards HER. Calculation the double layer capacitance at the solid-liquid interface based on CV is an alternative method to measure the relative effective active area. The capacitance of NiCoP/NF@NC is about 11.5 $mF\cdot cm^{-2}$, indicating a plenty of active sites in the NiCoP/NF@NC. The stability of NiCoP/NF@NC electrode was tested by CV scan between + 0.20 and –0.30 V *versus* RHE at a scan rate of 50 $mV\cdot s^{-1}$ in 1.0 $mol\cdot L^{-1}$ KOH electrolyte. As shown in Fig. 4(D), it is almost no degradation in current density and overpotential after continuous 10000 CV scanning, further confirming its excellent long-term electrochemical stability.

The polarization curves of OER performance of NiCoP/NF@NC was also tested in 1.0 $mol\cdot L^{-1}$ KOH at a scan rate of 5 $mV\cdot s^{-1}$, and the commercial RuO_2 catalyst coated on NF@NC (RuO_2-NF@NC) was also estimated for comparison. Figure 5(A) shows the LSV curves of NiCoP/NF@NC, NiP/NF@NC, CoP/NF@NC, NiCoP-NF@NC and RuO_2-NF@NC. The RuO_2-NF@NC exhibits a lowest overpotential of 210.4 mV at a current density of 10 $mA\cdot cm^{-2}$. NiCoP/NF@NC shows the higher current density at relative lower overpotential compared to other three electrodes. The NiCoP/NF@NC only demands a lower overpotential of 308.2 mV to achieve the current density of 10 $mA\cdot cm^{-2}$ compared to NiP/NF@NC (349.1

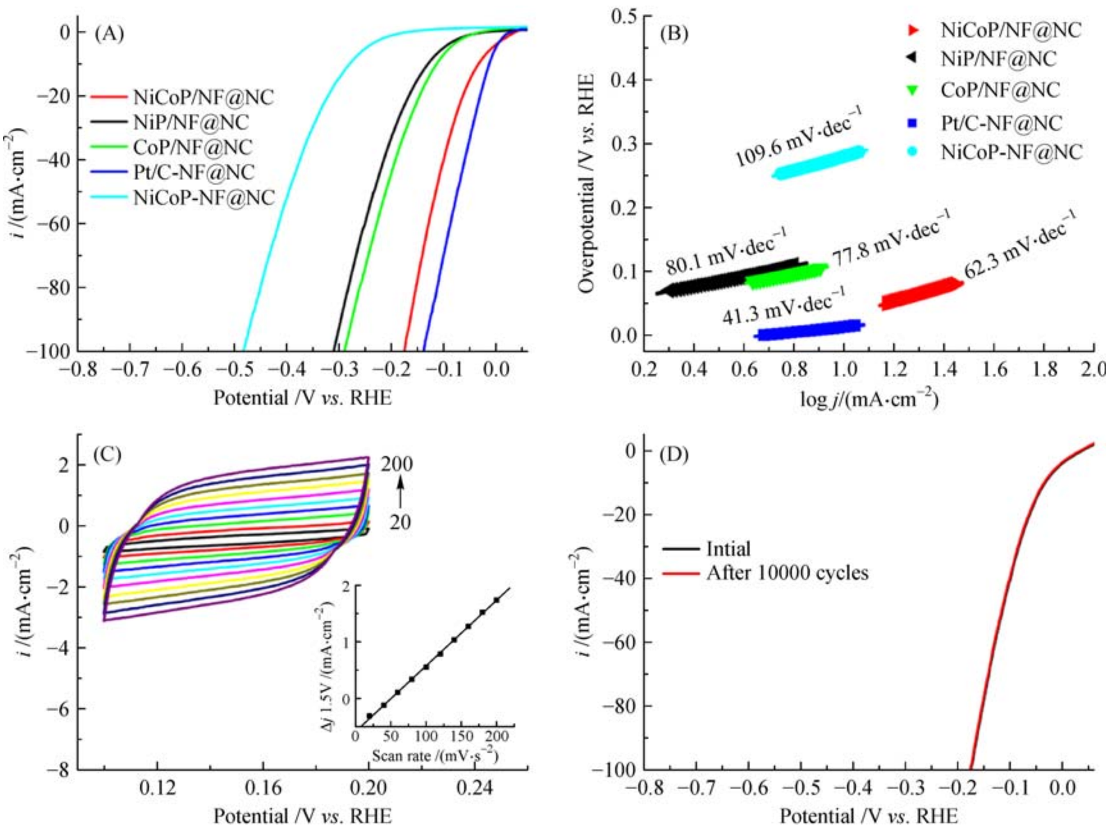

Fig. 4 (A) HER LSV curves of NiCoP/NF@NC, NiP/NF@NC, CoP/NF@NC, NiCoP-NF@NC and Pt/C-NF@NC in 1.0 mol·L^{-1} KOH electrolytes with a scan rate of 5 mV·s^{-1}; (B) corresponding Tafel slopes of the five catalysts; (C) electrochemical cyclic voltammogram of NiCoP/NF@NC at different scanning rates of 20−200 mV·s^{-1}, inset shows the corresponding C_{dl} obtained at 0.15 V *vs.* RHE; (D) LSV curves of NiCoP/NF@NC before and after continuous potential sweeps at a scan rate of 50 mV·s^{-1} in 1.0 mol·L^{-1} KOH electrolyte

mV), CoP/NF@NC (383.3 mV) and NiCoP-NF@NC (362.7 mV) (Table S2). Moreover, the previous study reported that the Ni_2P-CoP composites at 10 mA·cm^{-2} exhibit overpotentials of 105 mV for HER and 320 mV for OER [48], which are much higher than those of NiCoP/NF@NC. The synthetic NiCoP/NF@NC exhibits better performance towards HER and OER compared with the reported similar materials, such as NiCoP nanosheets and spheres [35,39]. It is further demonstrated the special structures of 3D network nanostructured NiCoP nanosheets enhance the electrocatalytic performance. As shown in Fig. 5(B), the Tafel slope for NiCoP/NF@NC is 94.5 mV·dec^{-1}, which is much lower than those for NiP/NF@NC (390.4 mV·dec^{-1}), CoP/NF@NC (394.9 mV·dec^{-1}), NiCoP-NF@NC (155.2 mV·dec^{-1}) and RuO_2-NF@NC (135.0 mV·dec^{-1}). This indicates that NiCoP/NF@NC has a more efficient OER electrocatalytic activity, and is even better than one of the best commercial RuO_2 catalysts, probably because the 3D network nanostructures facilitate the exposure of active sites, and the synergistic effect between N-doped carbon and network structured NiCoP may also be responsible for the superior OER activity.

Electrochemical impedance spectroscopy (EIS) was further used to study the electrode kinetics under the OER operating conditions as shown in Fig. 5(C). In the Nyquist plots, it is clearly revealed that the charge-transfer resistance is lower for the NiCoP/NF@NC electrode than for the NiP/NF@NC, CoP/NF@NC and NiCoP-NF@NC electrodes (Table S3), suggesting that NiCoP/NF@NC has the fastest charge transfer process. It is probably related to the good electrical contact between the NiCoP catalyst and NF@NC substrate derived from the *in-situ* growth strategy, resulting in the rapid electron transfer from the substrate to the catalyst surface. The long-term electrochemical stability is a critical criterion to estimate the electrocatalysts, and the 10000 cycles stability test results of NiCoP/NF@NC are shown in Fig. 5(D). Notably, after the 10000 cycles test, the LSV curve is almost coincident with the initial curve, indicating that no degradation happens during the long-term test. According to the previous studies, the surface-bound phosphates and phosphides of NiCoP can be oxidized to oxides or oxyhydroxides, and this is a common phenomenon for metal phosphides after OER catalysis [45,49]. Notably, the resulting NiCoP/Ni_xCo_yO (or Ni_xCo_yOOH) heterojunction could promote the OER activity by accelerating the electron transfer from the metallic NiCoP to the surface

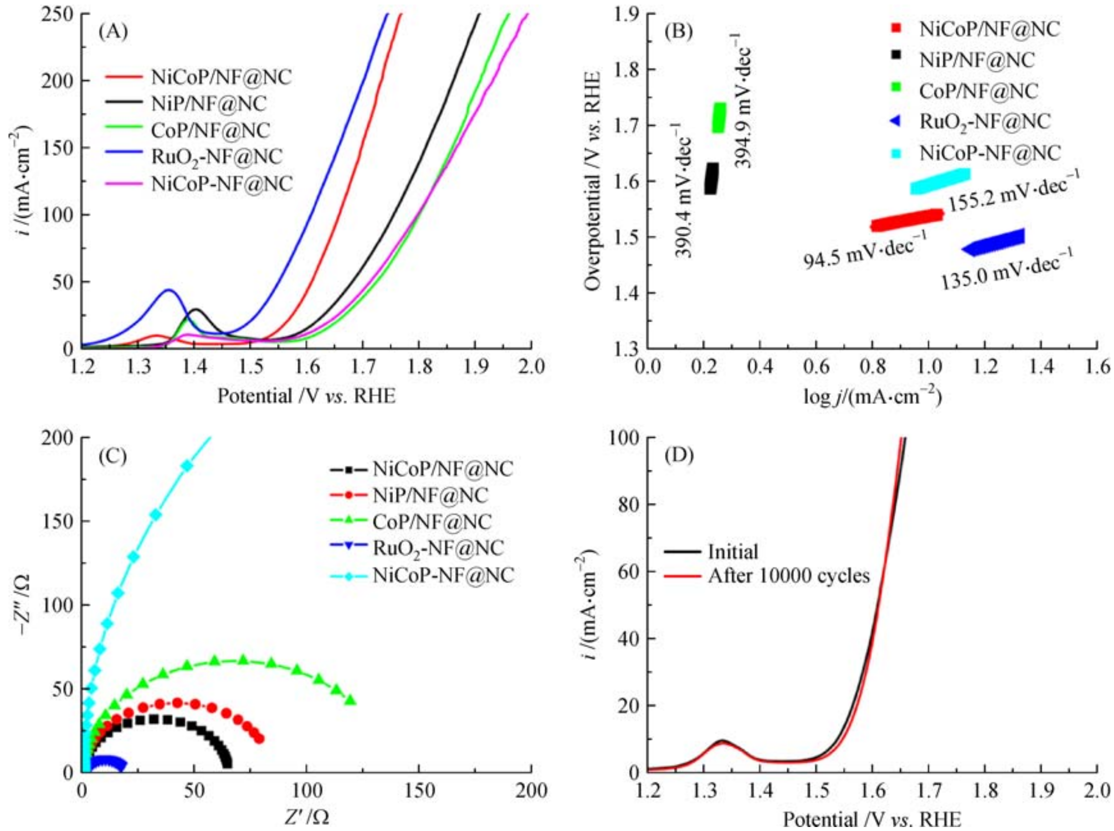

Fig. 5 (A) OER LSV curves of NiCoP/NF@NC, NiP/NF@NC, CoP/NF@NC, NiCoP-NF@NC and RuO_2-NF@NC in 1.0 mol·L^{-1} KOH electrolytes with a scan rate of 5 mV·s^{-1}; (B) corresponding Tafel slopes of the five catalysts; (C) EIS spectra for all the compared catalysts; (D) LSV curves of NiCoP/NF@NC before and after continuous potential sweeps at a scan rate of 50 mV·s^{-1} in 1.0 mol·L^{-1} KOH electrolyte

layer [50], resulting in the high activity and stability of NiCoP/NF@NC. The above results demonstrate that NiCoP/NF@NC is a good bifunctional electrocatalyst towards HER and OER.

4 Conclusions

A self-supported electrode composed of 3D network nanostructured NiCoP grown on N-doped carbon coated Ni foam (NiCoP/NF@NC) has successfully been synthesized by a hydrothermal route and a subsequent phosphorization process. The special structure has the following advantages: (i) 3D network structures could accelerate the diffusion of ions and improve the electrocatalytic performance; (ii) the N-doped carbon nanostructures could enhance the electrical conductivity and facilitate the transfer rate of electron; and (iii) the self-supported substrate could avoid the use of binder and enhance the performance. NiCoP/NF@NC can be used as an efficiency bifunctional electrocatalyst for both HER and OER in 1 mol·L^{-1} KOH electrolyte. NiCoP/NF@NC can reach a current density of 10 mA·cm^{-2} and has low overpotentials (31.8 mV for HER and 308.2 mV for OER), which are much better than the monometal catalysts of CoP/NF@NC and NiP/NF@NC. In addition, NiCoP/NF@NC also shows excellent long-term stability, as evidenced by that its performance has no obvious attenuation after 10000 time cycles. The present design strategy could be used for synthesis of bimetallic phosphide as a bifunctional electrocatalyst for water splitting.

Acknowledgements We gratefully acknowledge the support of this research by the National Natural Science Foundation of China (Grant Nos. 21631004 and 21771059), the Natural Science Foundation of Heilongjiang Province (No. B2017008), the University Nursing Program for Young Scholars with Creative Talents in Heilongjiang Province (No. UNPYSCT-2016016), the Harbin science and technology innovation talents research Foundation (No. 2015RAQXJ057).

Electronic Supplementary Material Supplementary material is available in the online version of this article at https://doi.org/10.1007/s11705-018-1711-1 and is accessible for authorized users.

References

1. Dresselhaus M S, Thomas I L. Alternative energy technologies. Nature, 2001, 414(6861): 332–337

2. Liu W, Hu E, Jiang H, Xiang Y, Weng Z, Li M, Fan Q, Yu X, Altman E I, Wang H. A highly active and stable hydrogen evolution catalyst based on pyrite-structured cobalt phosphosulfide. Nature Communications, 2016, 7: 10771
3. Jiao Y, Zheng Y, Davey K, Qiao S Z. Activity origin and catalyst design principles for electrocatalytic hydrogen evolution on heteroatom-doped graphene. Nature Energy, 2016, 1(10): 16130
4. Nφrskov J K, Bligaard T, Rossmeisl J, Christensen C H. Towards the computational design of solid catalysts. Nature Chemistry, 2009, 1(1): 37–46
5. Alapati S V, Johnson J K, Sholl D S. Using first principles calculations to identify new destabilized metal hydride reactions for reversible hydrogen storage. Physical Chemistry Chemical Physics, 2007, 9(12): 1438–1452
6. Zou X X, Zhang Y. Noble metal-free hydrogen evolution catalysts for water splitting. Chemical Society Reviews, 2015, 44(15): 5148–5180
7. Zhang B, Zheng X L, Voznyy O, Comin R, Bajdich M, García-Melchor M, Han L L, Xu J X, Liu M, Zheng L R, et al. Homogeneously dispersed, multimetal oxygen-evolving catalysts. Science, 2016, 352(6283): 333–337
8. Wang J H, Cui W, Liu Q, Xing Z C, Asiri A M, Sun X P. Recent progress in cobalt-based heterogeneous catalysts for electrochemical water splitting. Advanced Materials, 2016, 28(2): 215–230
9. Jin Y, Wang H, Li J, Yue X, Han Y, Shen P K, Cui Y, Jin Y S, Wang H T, Li J J, et al. Porous MoO_2 nanosheets as non-noble bifunctional electrocatalysts for overall water splitting. Advanced Materials, 2016, 28(19): 3785–3790
10. Feng L L, Yu G T, Wu Y Y, Li G D, Li H, Sun Y H, Asefa T, Chen W, Zou X X. High-index faceted Ni_3S_2 nanosheet arrays as highly active and ultrastable electrocatalysts for water splitting. Journal of the American Chemical Society, 2015, 137(44): 14023–14026
11. Chen Y Y, Zhang Y, Zhang X, Tang T, Luo H, Shuai N, Dai Z H, Wan L J, Hu J S. Self-templated fabrication of $MoNi_4/MoO_{3-x}$ nanorod arrays with dual active components for highly efficient hydrogen evolution. Advanced Materials, 2017, 29(39): 1703311
12. Guo X X, Kong R M, Zhang X P, Du H T, Qu F L. $Ni(OH)_2$ nanoparticles embedded in conductive microrod array: An efficient and durable electrocatalyst for alkaline oxygen evolution reaction. ACS Catalysis, 2017, 7(7): 4381–4385
13. Xu X J, Du P Y, Chen Z K, Huang M H. An electrodeposited cobalt-selenide-based film as an efficient bifunctional electrocatalyst for full water splitting. Journal of Materials Chemistry. A, Materials for Energy and Sustainability, 2016, 4(28): 10933–10939
14. Lee J E, Jang Y J, Xu W Q, Feng Z X, Park H Y, Kim J Y, Kim D H. PtFe nanoparticles supported on electroactive Au–PANI core@shell nanoparticles for high performance bifunctional electrocatalysis. Journal of Materials Chemistry. A, Materials for Energy and Sustainability, 2017, 5(26): 13692–13699
15. Feng J X, Wu J Q, Tong Y X, Li G R. Efficient hydrogen evolution on Cu nanodots-decorated Ni_3S_2 nanotubes by optimizing atomic hydrogen adsorption and desorption. Journal of the American Chemical Society, 2018, 140(2): 610–617
16. Feng J X, Xu H, Ye S H, Ouyang G F, Tong Y X, Li G R. Silica-polypyrrole hybrids as high-performance metal-free electrocatalysts for the hydrogen evolution reaction in neutral media. Angewandte Chemie-Internatioanal Edition, 2017, 56(28): 8120–8124
17. Feng J X, Xu H, Dong Y T, Lu X F, Tong Y X, Li G R. Efficient hydrogen evolution electrocatalysis using cobalt nanotubes decorated with titanium dioxide nanodots. Angewandte Chemie-Internatioanal Edition, 2017, 56(11): 2960–2964
18. Li J S, Wang Y, Liu C H, Li S L, Wang Y G, Dong L Z, Dai Z H, LiY F, Lan Y Q. Coupled molybdenum carbide and reduced graphene oxide electrocatalysts for efficient hydrogen evolution. Nature Communications, 2016, 7: 11204
19. Qin J S, Du D Y, Guan W, Bo X J, Li Y F, Guo L P, Su Z M, Wang Y Y, Lan Y Q, Zhou H C. Ultrastable polymolybdate-based metal organic frameworks as highly active electrocatalysts for hydrogen generation from water. Journal of the American Chemical Society, 2015, 137(22): 7169–7177
20. Tang Y J, Gao M R, Liu C H, Li S L, Jiang H L, Lan Y Q, Han M, Yu S H. Porous molybdenum-based hybrid catalysts for highly efficient hydrogen evolution. Angewandte Chemie-Internatioanal Edition, 2015, 54(44): 12928–12932
21. Li Z M, Han M, Xu D D, Yang J, Lin Y, Shi N E, Lu Y A, Yang R, Liu B T, Dai Z H, et al. Defect-rich Ni_3FeN nanocrystals anchored on N-doped graphene for enhanced electrocatalytic oxygen evolutionshulin. Advanced Functional Materials, 2018, doi: 10.1002/adfm.201706018
22. Deng D R, Xue F, Jia Y J, Ye J C, Bai C D, Zheng M S, Dong Q F. Co_4N nanosheet assembled mesoporous sphere as a matrix for ultrahigh sulfur content lithium-sulfur batteries. ACS Nano, 2017, 11(6): 6031–6039
23. Chen P Z, Xu K, Fang Z W, Tong Y, Wu J C, Lu X L, Peng X, Ding H, Wu C Z, Xie Y. Metallic Co_4N porous nanowire arrays activated by surface oxidation as electrocatalysts for the oxygen evolution reaction. Angewandte Chemie International Edition, 2015, 54(49): 14710–14714
24. Wan J, Wu J B, Gao X, Li T Q, Hu Z M, Yu H M, Huang L. Structure confined porous Mo_2C for efficient hydrogen evolution. Advanced Functional Materials, 2017, 27(45): 1703933
25. Zhou X F, Yang X L, Li H, Hedhili M N, Huang K W, Li L J, Zhang W J. Symmetric synergy of hybrid CoS_2-WS_2 electrocatalysts for the hydrogen evolution reaction. Journal of Materials Chemistry. A, Materials for Energy and Sustainability, 2017, 5(30): 15552–15558
26. Yu L, Yang J F, Lou X W. Formation of CoS_2 nanobubble hollow prisms for highly reversible lithium storage. Angewandte Chemie International Edition, 2016, 55: 13422–13426
27. Splendiani A, Sun L, Zhang Y, Li T, Kim J, Chim C Y, Galli G, Wang F. Emerging photoluminescence in monolayer MoS_2. Nano Letters, 2010, 10(4): 1271–1275
28. Li Y, Wang H, Xie L, Liang Y, Hong G, Dai H. MoS_2 nanoparticles grown on graphene: An advanced catalyst for the hydrogen evolution reaction. Journal of the American Chemical Society, 2011, 133(19): 7296–7299
29. Fang H, Chuang S, Chang T C, Takei K, Takahashi T, Javey A. High-performance single layered WSe_2 p-FETs with chemically doped contacts. Nano Letters, 2012, 12(7): 3788–3792
30. Ross J S, Klement P, Jones A M, Ghimire N J, Yan J, Mandrus D G, Taniguchi T, Watanabe K, Kitamura K, Yao W, et al. Electrically tunable excitonic light-emitting diodes based on monolayer WSe_2 p-

n junctions. Nature Nanotechnology, 2014, 9(4): 268–272

31. Kong D, Wang H, Cha J J, Pasta M, Koski K J, Yao J, Cui Y. Synthesis of MoS_2 and $MoSe_2$ films with vertically aligned layers. Nano Letters, 2013, 13(3): 1341–1347
32. Zhang Y, Chang T R, Zhou B, Cui Y T, Yan H, Liu Z K, Schmitt F, Lee J, Moore R, Chen Y L. Direct observation of the transition from indirect to direct bandgap in atomically thin epitaxial $MoSe_2$. Nature Nanotechnology, 2014, 9(2): 111–115
33. Park H, Zhang Y, Scheifers J P, Jothi P R, Encinas A, Fokwa B P T. Graphene- and phosphorene-like boron layers with contrasting activities in highly active Mo_2B_4 for hydrogen evolution. Journal of the American Chemical Society, 2017, 139(37): 12915–12918
34. Liang H, Gandi A N, Anjum D H, Wang X, Schwingenschllögl U, Alshareef H N. Plasma-assisted synthesis of NiCoP for efficient overall water splitting. Nano Letters, 2016, 16(12): 7718–7725
35. Li Y, Zhang H, Jiang M, Kuang Y, Sun X, Duan X. Ternary NiCoP nanosheet arrays: An excellent bifunctional catalyst for alkaline overall water splitting. Nano Research, 2016, 9(8): 2251–2259
36. He P, Yu X Y, Lou X W D. Carbon-incorporated nickel-cobalt mixed metal phosphide nanoboxes with enhanced electrocatalytic activity for oxygen evolution. Angewandte Chemie International Edition, 2017, 56(14): 3897–3900
37. Li J, Yan M, Zhou X, Huang Z Q, Xia Z, Chang C R, Ma Y, Qu Y. Mechanistic insights on ternary $Ni_{2-x}Co_xP$ for hydrogen evolution and their hybrids with graphene as highly efficient and robust catalysts for overall water splitting. Advanced Functional Materials, 2016, 26(37): 6785–679
38. Wang Z, Cao X, Liu D, Hao S, Du G, Asiri A M, Sun X. Ternary NiCoP nanosheet array on a Ti mesh: A high-performance electrochemical sensor for glucose detection. Chemical Communications, 2016, 52(100): 14438–14441
39. Wang C, Jiang J, Ding T, Chen G, Xu W, Yang Q. Monodisperse ternary NiCoP nanostructures as a bifunctional electrocatalyst for both hydrogen and oxygen evolution reactions with excellent performance. Advanced Materials Interfaces, 2016, 3(4): 1500454–1500458
40. Li J, Yan M, Zhou X, Huang Z Q, Xia Z, Chang C R, Ma Y, Qu Y. Mechanistic insights on ternary $Ni_{2-x}Co_xP$ for hydrogen evolution and their hybrids with graphene as highly efficient and robust catalysts for overall water splitting. Advanced Functional Materials, 2016, 26(37): 6785–6796
41. Liu Q, Tian J, Cui W, Jiang P, Cheng N, Asiri A M, Sun X. Carbon nanotubes decorated with CoP nanocrystals: A highly active non-noble-metal nanohybrid electrocatalyst for hydrogen evolution. Angewandte Chemie International Edition, 2014, 53(26): 6710–6714
42. Yuan C, Li J, Hou L, Zhang X, Shen L, Lou X W D. Ultrathin mesoporous $NiCo_2O_4$ nanosheets supported on Ni foam as advanced electrodes for supercapacitors. Advanced Functional Materials, 2012, 22(21): 4592–4597
43. Yuan C Z, Yang L, Hou L R, Shen L F, Zhang X G, Lou X W. Growth of ultrathin mesoporous Co_3O_4 nanosheet arrays on Ni foam for high-performance electrochemical capacitors. Energy & Environmental Science, 2012, 5(7): 7883–7887
44. Yu L, Zhang G, Yuan C, Lou X W D. Hierarchical $NiCo_2O_4$@MnO_2 core-shell heterostructured nanowire arrays on Ni foam as high-performance supercapacitor electrodes. Chemical Communications, 2013, 49(2): 137–139
45. Du C, Yang L, Yang F L, Cheng G Z, Luo W. Nest-like NiCoP for highly efficient overall water splitting. ACS Catalysis, 2017, 7(6): 4131–4137
46. Du D H, Li P C, Ouyang J Y. Nitrogen-doped reduced graphene oxide prepared by simultaneous thermal reduction and nitrogen doping of graphene oxide in air and its application as an electrocatalyst. ACS Applied Materials & Interfaces, 2015, 7(48): 26952–26958
47. Zheng J, Chen X L, Zhong X, Li S Q, Liu T Z, Zhuang G L, Li X N, Deng S W, Mei D H, Wang J G. Hierarchical porous NC@CuCo nitride nanosheet networks: Highly efficient bifunctional electrocatalyst for overall water splitting and selective electrooxidation of benzyl alcohol. Advanced Functional Materials, 2017, 27(46): 1704169
48. Liang X, Zheng B, Chen L, Zhang J, Zhuang Z, Chen B. MOF-derived formation of Ni_2P-CoP bimetallic phosphides with strong interfacial effect toward electrocatalytic water splitting. ACS Applied Materials & Interfaces, 2017, 9(27): 23222–23229
49. Liang H, Gandi A N, Anjum D H, Wang X, Schwingenschlögl U, Alshareef H N, Ngenschlögl U S, Alshareef H N. Plasma-assisted synthesis of NiCoP for efficient overall water splitting. Nano Letters, 2016, 16(12): 7718–7725
50. Wang X, Li W, Xiong D, Petrovykh D Y, Liu L. Bifunctional nickel phosphide nanocatalysts supported on carbon fiber paper for highly efficient and stable overall water splitting. Advanced Functional Materials, 2016, 26(23): 4067–4077